Influence of viscoelastic and viscous absorption on ultrasonic wave propagation in cortical bone: Application to axial transmission

Salah Naili[a] and Mai-Ba Vu
Laboratoire Modélisation et Simulation Multi-Échelle, Université Paris-Est, UMR 8208 CNRS, 94010 Créteil Cédex, France

Quentin Grimal and Maryline Talmant
UPMC Univiversité Paris 6, UMR 7623 CNRS, LIP, F-75005 Paris, France and Laboratoire d'Imagerie Paramétrique, F-75005 Paris, France

Christophe Desceliers and Christian Soize
Laboratoire Modélisation et Simulation Multi-Échelle, Université Paris-Est, UMR 8208 CNRS, 77454 Marne la Vallée Cédex 2, France

Guillaume Haïat
Laboratoire de Recherches Orthopédiques, Université Paris 7, UMR 7052 CNRS, B2OA, 75010 Paris, France

(Received 24 July 2009; revised 6 February 2010; accepted 9 February 2010)

Cortical bone and the surrounding soft tissues are attenuating and heterogeneous media, which might affect the signals measured with axial transmission devices. This work aims at evaluating the effect of the heterogeneous acoustic absorption in bone and in soft tissues on the bone ultrasonic response. Therefore, a two-dimensional finite element time-domain method is derived to model transient wave propagation in a three-layer medium composed of an inhomogeneous transverse isotropic viscoelastic solid layer, sandwiched between two viscous fluid layers. The model couples viscous acoustic propagation in both fluid media with the anisotropic viscoelastic response of the solid. A constant spatial gradient of material properties is considered for two values of bone thicknesses (0.6 and 4 mm). In the studied configuration, absorption in the surrounding fluid tissues does not affect the results, whereas bone viscoelastic properties have a significant effect on the first arriving signal (FAS) velocity. For a thin bone, the FAS velocity is governed by the spatially averaged bone properties. For a thick bone, the FAS velocity may be predicted using a one-dimensional model. © *2010 Acoustical Society of America.* [DOI: 10.1121/1.3353091]

PACS number(s): 43.80.Ev, 43.20.Mv, 43.20.Px, 43.40.Rj [CCC] Pages: 2622–2634

I. INTRODUCTION

Different metabolic diseases such as osteoporosis may affect bone quality (WHO Study Group, 1994), resulting in a decrease in bone mass and micro-architectural deterioration of bone tissue, which implies an increase in bone fragility. The diaphysis of long bones such as radius and femur is mainly constituted of cortical bone. Investigating cortical bone quality is of interest (Rico, 1997) because it accounts for about 80% of the skeleton, supports most of the load of the body, and is mainly involved in osteoporotic fractures (Seeley *et al.*, 1991). Moreover, cortical bone quality has recently been shown to be determinant for bone mechanical stability (Mayhew *et al.*, 2005) at the femur neck.

In axial transmission (AT) technique (which is particularly adapted to cortical long bone evaluation), both ultrasound emitter and receivers, are placed in the same side of the investigated skeletal site, along a direction close to the long bone axis. The earliest event or wavelet (usually called first arriving signal, FAS) of the multicomponent signal recorded by the receivers has been the most widely investigated. The wave velocity associated with this signal, which is measured in the time domain, can be used to discriminate healthy subjects from osteoporotic patients, and is therefore considered as a relevant index of bone status (Hans *et al.*, 1999; Muller *et al.*, 2005; Stegman *et al.*, 1995; Talmant *et al.*, 2009; Weiss *et al.*, 2000). Both experimental (Bossy *et al.*, 2004c; Raum *et al.*, 2005) and simulation studies (Bossy *et al.*, 2004b) have shown that the FAS velocity was related to different bone properties (bone mineral density, cortical thickness and bone elastic properties). Numerical simulations have been employed to show that when the cortical thickness is comparable or larger than the wavelength, the type of wave contributing to the FAS corresponds to a lateral wave, whereas when the wavelength is larger than the cortical thickness divided by four, the received signal corresponding to the FAS comes from the first symmetric Lamb wave mode (S_0) guided by the cortical thickness (Bossy *et al.*, 2002).

Cortical bone is a complex medium from a biomechanical point of view. Its elastic behavior has been described as transverse isotropic in different works (Dong and Guo, 2004;

[a]Author to whom correspondence should be addressed. Electronic mail: salah.naili@univ-paris-est.fr

 0001-4966/2010/127(4)/2622/13/$25.00

Haïat *et al.*, 2009). At the macroscopic scale, porosity in the radial direction (which is associated with the cross-section of the bone) is heterogeneous at all ages and for both genders (Bousson *et al.*, 2001; Thomas *et al.*, 2005): the mean porosity in the endosteal region (inner part of the bone) is significantly higher than in the periosteal region (outer part of the bone). Moreover, cortical bone is affected by age-related bone resorption and osteoporosis. It undergoes a thinning of the cortical shell, as well as an increase in porosity, mainly in the endosteal region (Bousson *et al.*, 2001). An increase in porosity is likely to affect bone material properties (mass density and elasticity) (Fritsch and Hellmich, 2007), which may in turn impact bone quality (Ammann and Rizzoli, 2003). Similarly, a thinning of the cortical shell is an important indicator of decreasing bone strength and of fracture risk (Turner, 2002). Moreover, cortical bone is a strongly attenuating medium where ultrasonic propagation occurs with losses (Han *et al.*, 1996; Lakes *et al.*, 1986; Langton *et al.*, 1990; Lees and Klopholz, 1992; Serpe and Rho, 1996). Ultrasonic attenuation may be due to the viscoelastic behavior of the bone matrix, as well as to the presence of the pores (through scattering effects of the ultrasonic wave) (Sasso *et al.*, 2007, 2008). The feasibility of frequency dependent attenuation coefficient measurements has been demonstrated in bovine cortical bone samples of a scale of the centimeter (Sasso *et al.*, 2007). Interestingly, broadband ultrasonic attenuation (BUA, defined as the slope of the curve of the frequency dependent attenuation coefficient) measurements have recently been shown to be significantly related to the microstructure, as well as to bone physical properties such as mass and bone mineral densities (Sasso *et al.*, 2008). Therefore, BUA has been evoked as a suitable parameter for cortical bone quality estimation. Similarly, human soft tissues such as skin, fat, and muscles (between the transducers and bone) or bone marrow (inside cortical bone) are also media where ultrasonic attenuation has been measured.

The potential advantage of numerical simulation tools over experimental approaches is that it can be used to determine the influence of each bone property independently, which is difficult when working with real samples, as all bone geometrical and mechanical properties evolve in parallel. Modeling the FAS in AT experiment is a time-domain elasto-acoustic problem. Time-domain analytical methods have been used in the past to solve the elasto-acoustic wave system in simple AT models (Grimal and Naili, 2006; Macocco *et al.*, 2005, 2006). Bossy *et al.* (2004b) have assessed the influence of a gradient of longitudinal wave velocity due to a heterogeneous distribution of porosity on the FAS velocity. More recently, our group has determined [using the COMSOL Multiphysics software (COMSOL Multiphysics, 2005)] the effect of heterogeneous material bone properties on the ultrasonic response, and more specifically, on the FAS velocity using 2-D finite element model (FEM) (Haïat *et al.*, 2009). Most models of AT developed in the past have considered cortical bone and the surrounding soft tissues as an elastic material. However, the influence of ultrasonic attenuation (in bone and/or in the surrounding soft tissues) on the ultrasonic response of the investigated anatomical site in the framework of the AT device remains unclear. Studying the influence of attenuation in bone on the FAS velocity is of particular interest since BUA has been suggested as a potential indicator of bone status. In addition, the determination of the sensitivity of the ultrasonic response of bone to attenuation variations may be considered as a first step toward the resolution of the inverse problem.

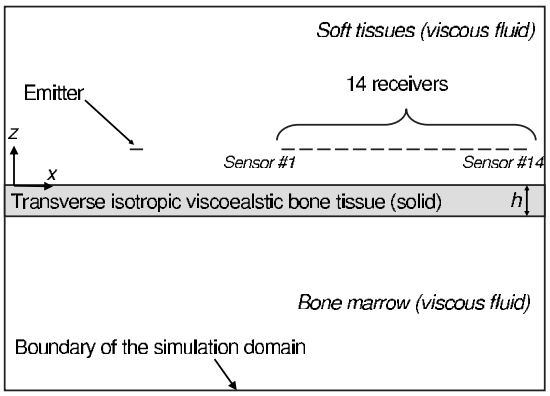

FIG. 1. Schematic representation of the simulation domain corresponding to a three-layer medium. The emitter and receivers are indicated by indents.

The aim of this paper is to assess the effect of the viscoelastic nature of cortical bone and of the viscous nature of the surrounding soft tissues on the ultrasonic response obtained with an AT device. Here, bone is modeled as an anisotropic (transverse isotropic) heterogeneous (a gradient of material properties in the radial direction is considered) viscoelastic material, and the surrounding soft tissues are modeled as homogeneous viscous liquids. More specifically, we aim at investigating the potentiality of 2-D finite element numerical simulation tools to assess the sensitivity of the FAS velocity to variations of different viscoelastic parameters.

With this introduction as background, a 2-D finite element model briefly described in Sec. II is used to compute the dependence of the FAS velocity on all viscoelastic coefficients of cortical bone at the organ level, as well as on the viscous nature of the surrounding soft tissues. The models used for the viscoelastic tensor are presented and discussed. Section III describes (i) the sensitivity of the FAS velocity to changes of each viscoelastic coefficient for homogeneous material properties, (ii) the effect of a constant gradient of each viscoelastic coefficient affecting the FAS velocity, and (iii) the effect of a constant gradient of porosity. Results are then discussed in Sec. IV.

II. METHOD

A. Simulation of the axial transmission configuration

The geometrical configuration used in the present study is the same as the one used by Haïat *et al.* (2009), and readers are referred to this previous study for details on the configuration. Briefly, cortical bone is modeled as a two-dimensional multilayer medium composed of one heterogeneous viscoelastic transverse isotropic solid layer, sandwiched between two homogeneous viscous fluid layers, as shown in Fig. 1. The cortical thickness is denoted h and the direction z corresponds to the bone radial direction.

In the simulation, a pressure source is positioned in the fluid and the excitation signal is a Gaussian pulse with a center frequency of 1 MHz, identical to the one given and plotted by Desceliers *et al.* (2008). The geometrical arrangement shown in Fig. 1 mimics that of the probe developed by the "Laboratoire d'Imagerie Paramétrique" (France) (Bossy *et al.*, 2004a). The FAS velocity is then determined following the procedure used in experiments with the actual probe (Bossy *et al.*, 2004a). Signals are collected for each one of the 14 receivers located in the soft tissue. The time t_i of the first maximum of each of the 14 signals recorded at the sensor #i was then determined using a thresholding method. The FAS velocity estimate is then given by the slope of the position of each sensor #i versus t_i, obtained through a least-square linear regression.

Moreover, we also consider the dependence of the amplitude of the first maximum of the signal recorded at the sensor #i as function of i, in order to assess the effect of viscoelasticity on the amplitude of the FAS.

In both fluid media, the formulation is written in terms of pressure. The equation of propagation in the viscous fluid is given by

$$\rho_f \ddot{p} = \eta_f \Delta \dot{p} + K \Delta p, \tag{1}$$

where $p(\mathbf{x};t)$ denotes the pressure field, ρ_f mass density, K the fluid compressibility, and η_f the bulk viscosity of the fluid. The acoustic wave velocity c_f in absence of viscosity ($\eta_f=0$) is given by $c_f=\sqrt{K/\rho_f}$.

In the solid media, the formulation is written in terms of displacement. Neglecting body forces, the momentum conservation equation writes

$$\text{div}\ \boldsymbol{\sigma} = \rho_s \ddot{\mathbf{u}}, \tag{2}$$

where $\boldsymbol{\sigma}(\mathbf{x};t)$ is the stress tensor, ρ_s is the bone mass density, and $\mathbf{u}(\mathbf{x};t)$ is displacement vector.

Cortical bone is modeled as an heterogeneous material using the linear theory of viscoelastic without memory. In this theory, the stress tensor $\boldsymbol{\sigma}$ is linearly related to the strain tensor $\boldsymbol{\epsilon}(\mathbf{x};t)$ and to the rate-of-deformation tensor $\dot{\boldsymbol{\epsilon}}(\mathbf{x};t)$

$$\boldsymbol{\sigma} = \mathbb{C}\boldsymbol{\epsilon} + \mathbb{E}\dot{\boldsymbol{\epsilon}}, \tag{3}$$

where $\mathbb{C}(\mathbf{x})$ is the stiffness tensor and $\mathbb{E}(\mathbf{x})$ is the viscoelastic tensor. For a 2-D transverse isotropic medium (in the plane defined by (x,z)), the stiffness tensor writes

$$\mathbb{C} = \begin{pmatrix} C_{11}(z) & C_{13}(z) & 0 \\ C_{13}(z) & C_{33}(z) & 0 \\ 0 & 0 & C_{55}(z) \end{pmatrix}, \tag{4}$$

where all stiffness coefficients only depend on z because only the heterogeneity in the radial direction is modeled, similarly as what was done by Haïat *et al.* (2009).

Cortical bone has been shown to be a significantly anisotropic medium in terms of ultrasonic attenuation, as BUA values measured in the axial direction are significantly smaller than BUA values obtained in the radial and tangential directions (Lakes *et al.*, 1986; Lees and Klopholz, 1992; Sasso *et al.*, 2007). Therefore, we have considered an anisotropic (transverse isotropic) tensor $\mathbb{E}$ to describe the bone dissipative behavior. In order to retrieve a physiological range of variation for the attenuation in cortical bone, we have used a study carried out with bovine cortical bone samples (Sasso *et al.*, 2007) because we could not find in the literature a sufficient amount of data in human cortical.

Moreover, BUA values depend significantly on bone mineral density and on mass density (Sasso *et al.*, 2008), which are two quantities closely related to the porosity. As the spatial distribution of porosity is heterogeneous in cortical bone (Bousson *et al.*, 2001), the viscoelastic properties of cortical bone are also expected to be spatially dependent. Therefore, we have considered an heterogeneous behavior of the viscoelastic tensor $\mathbb{E}$, similar to the one given in Eq. (4), and the viscoelastic tensor $\mathbb{E}$ writes

$$\mathbb{E} = \begin{pmatrix} \eta_{11}(z) & \eta_{13}(z) & 0 \\ \eta_{13}(z) & \eta_{33}(z) & 0 \\ 0 & 0 & \eta_{55}(z) \end{pmatrix}, \tag{5}$$

where all viscoelastic coefficients, written using the Voigt notation, only depend on z.

The boundary conditions at the edges of the simulation domain are identical to the one used by Desceliers *et al.* (2008). At both interfaces between the fluid layers and the solid layer, the boundary conditions in terms of displacement and normal stresses are taken into account. The model therefore fully describes the fluid-structure interaction between the three sub-domains. For each computation, around 186 000 triangular elements are used, resulting in about 393 000 degrees of freedom. The simulation software is the 3.5 version of COMSOL Multiphysics (2005).

The physiological variations of the different material properties are indicated in Appendix.

B. Lamb and bulk wave modes

When the thickness h is smaller than the wavelength λ (typically $h/\lambda < 0.25$), the FAS velocity tends toward the so-called plate velocity, which is the phase velocity of the first symmetric Lamb wave mode S_0 in the large wavelength limit (Bossy *et al.*, 2002, 2004b; Haïat *et al.*, 2009), with the expression

$$v_p = \sqrt{\frac{C_{11}}{\rho_s} \times \left(1 + \frac{C_{13}^2}{C_{11} \times C_{33}}\right)}, \tag{6}$$

which is only valid in the case of an elastic material.

When the thickness h is large compared to wavelength, the FAS velocity tends toward the bulk longitudinal wave velocity inside the material constituting the solid layer:

$$v_b = \sqrt{\frac{C_{11}}{\rho_s}}, \tag{7}$$

which is again only valid in the case of an elastic material.

In the present study, simulations were performed with two different solid layer thicknesses, $h=0.6$ mm and $h=4$ mm, because these two values of h correspond to cases where the behavior of the FAS velocity can be explained in terms of guided and bulk waves, respectively. Considering the dominant frequency of the broadband ultrasonic pulse

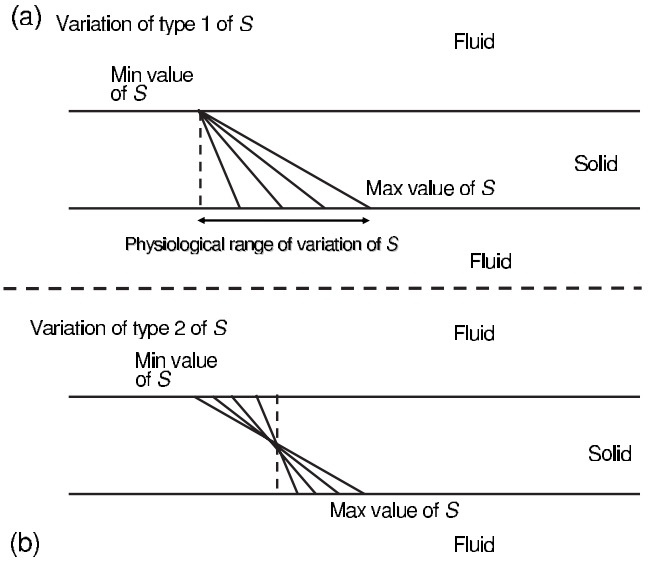

FIG. 2. Schematic representation of the two types of spatial variation considered for the material property S corresponding the viscoelastic coefficient. The lines in the solid layer indicate the spatial dependence of S. The dotted line indicates homogeneous material properties corresponding the reference material properties. The variation in type 1 (respectively, 2) shown in (a) [respectively, (b)] corresponds to a constant value at the bone-soft tissues interface (respectively in the middle of the bone).

and the range of variation in C_{11}, it means that h/λ varies in the intervals defined from 0.14 to 0.19, and from 0.96 to 1.25, respectively, for the thin and thick solid layers.

For the thinnest layer, the propagation in the solid layer is analyzed on the basis of the propagation of S_0 wave in an immersed homogeneous plate after adjustment of the material properties. Therefore, roots associated with the characteristic equation of the S_0 wave for homogenous transverse isotropic plate are calculated in the limit of large wavelengths.

C. Gradient of material property

Similarly, as what was done by Haïat *et al.* (2009), the impact of a controlled gradient vector $\boldsymbol{\delta}$ of a given material property S on the FAS velocity is investigated. In what follows, the scalar S corresponds to one of the viscoelastic coefficients η_{ij} defined in Eq. (5). In each set of simulations, all the material properties (stiffness and viscoelastic coefficients) are constant and equal to their reference value, while S is subjected to a gradient defined below.

The gradient vector $\boldsymbol{\delta}=\text{grad}\, S=\delta\mathbf{z}$ is assumed to be independent of x in all cases, where $\mathbf{z}$ is a unit vector along the z-axis and grad is the gradient operator acting on a scalar field. The quantity δ is always taken as negative because attenuation increases with porosity (Sasso *et al.*, 2008), and porosity is higher in the endosteal part than in the periosteal part of the bone. Moreover, only the simple situation of affine spatial variations of S is considered, corresponding to a constant value of δ. This affine spatial variation in S is chosen because the actual physiological spatial dependence of S remains unknown. Two different affine spatial dependences of the studied viscoelastic property are considered and are illustrated in Fig. 2. The associated gradient δ will be referred to as type 1 or 2, and corresponds to simple description of the spatial dependence of material properties. We choose this linear variation because the precise spatial variations of bone material properties remain poorly documented.

Type 1. The gradient of type 1 is such that the physical property S takes the same value S_m at the upper interface $z=0$ of the solid plate for all values of the gradient δ. The quantity $S(z)$ is therefore given by

$$S(z) = S_m + \delta \times z, \tag{8}$$

where S_m corresponds to the minimal value of the material property S considered. The minimal value δ_m of δ (which corresponds to its maximum in absolute value as $\delta<0$) is chosen so that $S(-h)$ is equal to S_M, where S_M is the maximal value of S. The gradient δ_m is given by

$$\delta_m = \frac{(S_m - S_M)}{h} < 0. \tag{9}$$

Type 2. The gradient of type 2 is such that S takes the same value at the middle of the solid plate ($z=-h/2$) for all values of gradient δ. Furthermore, the mean value of the property S is identical for all δ, and the quantity $S(z)$ is given by

$$S(z) = \frac{(S_m + S_M)}{2} + \delta \times \left(z + \frac{h}{2}\right). \tag{10}$$

The minimal value of δ is also given by Eq. (9) so that all values of $S(z)$ are again always comprised between S_m and S_M.

For both types of spatial variation, five different values of δ regularly distributed between δ_m and 0 are arbitrarily considered for each layer thickness. In what follows, the notations δ_{11}, δ_{13}, δ_{33}, and δ_{55} correspond to δ when S is defined by η_{11}, η_{13}, η_{33}, and η_{55}, respectively.

D. Gradient of porosity

In the case of bone, all material properties (mass density, stiffness, and viscoelastic coefficients) are expected to exhibit coupled spatial variations because they are all related to porosity, which increases from the periosteal to the endosteal part (Bousson *et al.*, 2001). When porosity increases, the values of the homogenized elastic constants and of mass density are expected to decrease, having opposite and competing effects on the wave velocity. In addition, the viscoelastic constants are expected to increase with porosity (Sasso *et al.*, 2008). Here, spatial variations of types 1 and 2 are considered for the porosity (noted P), with the minimum and maximum values of porosity P_m and P_M equal, respectively, to 3 and 15%. In the case of a spatial variation in types 1 and 2, the porosity writes, respectively,

$$P(z) = P_M + \delta_P \times z, \tag{11}$$

$$P(z) = \frac{(P_m + P_M)}{2} + \delta_P \times \left(z + \frac{h}{2}\right). \tag{12}$$

The dependence of mass density and of the stiffness coefficients is similar to what has been done by Haïat *et al.*

(2009), and is briefly recalled in what follows. Following a simple rule of mixture, a variation in porosity induces an affine variation in mass density given by

$$\rho_s(z) = \rho_m + \delta_\rho \times (P-3). \quad (13)$$

Here, we choose ρ_m in order to obtain a variation in mass density from 1.753 to 1.66 g cm^{-3} when P varies from 3% and 15%, which leads to $\delta_\rho = 7.7 \times 10^{-3}$ g cm^{-3}. These values correspond to a mass density equal to 1.722 g cm^{-3} when $P=7\%$.

The variations in all material properties with porosity are taken from the literature. Affine dependence of diagonal components of $\mathbb{C}$ with porosity was derived from Baron *et al.* (2007), where a variation of porosity between 3% and 15% corresponds approximately to a change of C_{11} and C_{33} of 7.8 and 4 GPa, respectively,

$$C_{11}(z) = C_{11}^m + \delta_C \times (P-3), \quad C_{33}(z) = C_{33}^m + \delta'_C \times (P-3). \quad (14)$$

The variations of C_{11} and C_{33} are centered on their reference value. Therefore, C_{11}^m and C_{33}^m are respectively equal to 19.7 and 16.85 GPa; the quantities δ_C and δ'_C are respectively equal to 0.65 and 0.33 GPa. Note that taking into account a slight nonlinear variation in C_{11} and C_{33} as a function of porosity should not modify significantly our results. Similarly as what was done by Haïat *et al.* (2009), we did not consider any variation in C_{13}, which was taken to be equal to its reference value.

Although BUA has been shown to increase when mass density and bone mineral density (which are both negatively correlated with porosity) decrease (Sasso *et al.*, 2008), the precise relationship between porosity and attenuation remains unknown. Therefore, for each viscoelastic constant η_{ij}, we assume (i) a linear relation between the corresponding attenuation at 1 MHz and porosity, and (ii) that the ultrasonic attenuation value at P_m (respectively P_M) corresponds to its minimal (respectively maximal) value within the physiological range. This approach constitutes a simple mean of investigating the effect of viscoelasticity variations due to heterogeneous porosity.

III. RESULTS

A. Physiological material properties

The same approach as the one described by Haïat *et al.* (2008a) is used to derive the attenuation coefficient α_f in bone marrow (see Appendix). We assumed that the bone marrow viscosity is similar to that of soft tissues, and the range of variation used for α_f is shown in Table I. The corresponding values of η_f were obtained using Eq. (A2).

TABLE I. Mean, maximum, and minimum values of the attenuation coefficient at 1 MHz and of the corresponding viscosity of bone marrow and of soft tissues considered in the present study. These values are taken from Dussik and Fritch (1956); Goss *et al.* (1978); Lehman and Johnson (1958).

Physical property	α_f (1 MHz) (dB cm^{-1})	η_f (Pa s)
Mean value (reference)	1	1.97
Minimum value	0	0
Maximum value	2	3.94

TABLE II. Mean, maximum, and minimum values of the four homogenized elastic constants and of mass density affecting the ultrasonic propagation in the framework of the 2D model of Fig. 1.

Mechanical quantity	C_{11} (GPa)	C_{13} (GPa)	C_{33} (GPa)	$C_{55}=G_L$ (GPa)	ρ_s (g cm^{-3})
Mean value (reference)	23.05	8.7	15.1	4.7	1.722
Minimum	17.6	5.1	11.8	3.3	1.66
Maximum	29.6	11.1	25.9	5.5	1.753

The values used for the stiffness tensor of cortical bone are the same as the ones given by Haïat *et al.* (2009) and are shown in Table II.

The values of the longitudinal attenuation coefficients associated with the axial and radial directions ($\alpha_{L,x}$ and $\alpha_{L,z}$, respectively) at 1 MHz were obtained from the axial and radial BUA values, respectively, assuming a linear frequency dependence of the attenuation coefficients within the entire frequency bandwidth. The mean value of the attenuation coefficient α_t (see Appendix) indicated in Table III was taken from Garcia *et al.* (1978). The corresponding value of η_{55} was obtained using Eq. (A5) by considering the reference values of the material properties indicated in Table II.

B. Analytical validation of the finite element model

In order to validate our simulation code in the framework of a viscoelastic constitutive law, the results obtained numerically in a simple geometrical situation (planar propagation) are compared to analytical results. Therefore, a through transmission experiment was simulated using the numerical simulation tool in order to verify that the material properties used as input parameters could be retrieved by analyzing the simulation results. Briefly, a 2-D plane wave propagation was considered in a rectangular simulation domain (10×5 mm^2) in the x-axis. A linear emitter was positioned at $x=0$, generating a broadband ultrasonic signal similar to that described by Desceliers *et al.* (2008). A linear receiver is located at the other end of the simulation domain (at $x=10$ mm) to record the ultrasonic wave after its propa-

TABLE III. Average, minimum, and maximum values of attenuation and corresponding viscoelastic coefficient taken for cortical bone. The values of $\alpha_{L,x}$ and $\alpha_{L,z}$ were taken from Table 1 of Sasso *et al.* (2007). The mean value of α_T was taken from Garcia *et al.* (1978). The corresponding values of η_{55} was obtained using Eq. (A5) by considering the reference values of the material properties indicated in Table II. The mean value of η_{13} was obtained using Eq. (A7) and the maximum and minimum values of η_{13} were obtained by verifying that the thermodynamical stability condition given by Eq. (A8) is always respected when η_{11} and η_{33} vary within their physiological range.

Mechanical quantity	$\alpha_{L,x}$ (dB cm^{-1})	$\alpha_{L,z}$ (dB cm^{-1})	α_T (dB cm^{-1})	η_{11} (Pa s)	η_{33} (Pa s)	η_{55} (Pa s)	η_{13} (Pa s)
Mean value (reference)	3.2	4.2	4	157	109	18	121
Minimum	0.8	1.7	0	39	44	0	39
Maximum	10.6	12.8	8	521	334	36.2	131

gation in the viscoelastic domain where the stiffness (respectively viscoelastic) coefficients correspond to the mean values indicated in Table II (respectively Table III). Longitudinal and transverse wave modes were successively tested by considering a time-dependent displacement in the x and z directions at the emitter as boundary conditions.

Meanwhile, the propagation of a longitudinal ultrasonic wave in water was simulated using the formulation in terms of pressure, leading to the reference signal, which is similar in shape to the input signal (data not shown). The reference signal is necessary in the framework of a through transmission configuration to derive the phase velocity. The black solid lines in Figs. 3(a) and 3(b) [respectively Figs. 3(c) and 3(d)] show the behavior of the frequency dependent attenuation coefficient (respectively of the phase velocity) within the frequency bandwidth of interest, obtained using the ratio of the spectra of the reference signal and of the signal transmitted in the simulation domain for the longitudinal and transverse wave modes (Haïat *et al.*, 2008b; Sasso *et al.*, 2008).

These last simulation results were compared to analytical results obtained by considering a plane wave propagation in a viscoelastic medium under the same assumptions of relatively weak absorption given in Appendix3, where (i) the attenuation coefficient varies has a f-square dependence, as indicated by Eqs. (A3) and (A5), and (ii) the longitudinal and transverse phase velocities $v_{L,x}^{\phi}$ and v_T^{ϕ} vary as a second order polynomial as a function of frequency, as indicated by Eqs. (A4) and (A6). The gray dashed lines in Fig. 3 show the frequency dependences of the attenuation coefficient and of phase velocity obtained using the analytical model described above. A good agreement between analytical and numerical results is obtained for the frequency dependences of $\alpha_{L,x}$ and α_T as the maximum difference between the two results is equal to 0.01 dB cm^{-1} for $\alpha_{L,x}$ and 0.012 dB cm^{-1} for α_T. Slightly more important discrepancies are obtained between the analytical and the numerical results for the frequency dependence of phase velocity as the difference between the two results slightly increases with frequency, and its maximum value is equal to 0.7 m s^{-1} for $v_{L,x}^{\phi}$ and to 0.3 m s^{-1} for v_T^{ϕ}. These discrepancies may be explained by effects related to numerical error in the scheme of the spatio-temporal discretization, which have been pointed out for example in Warren and Scott (1996), and are known to be due to the discretization. This numerical error is not due to the distortion effects during the pulse propagation related to dispersion, which has been detailed by Haïat *et al.* (2006) when the velocity is measured using a time marker such as the first zero crossing. Figure 3 thus constitutes a validation of the simulation method and an estimation of the error.

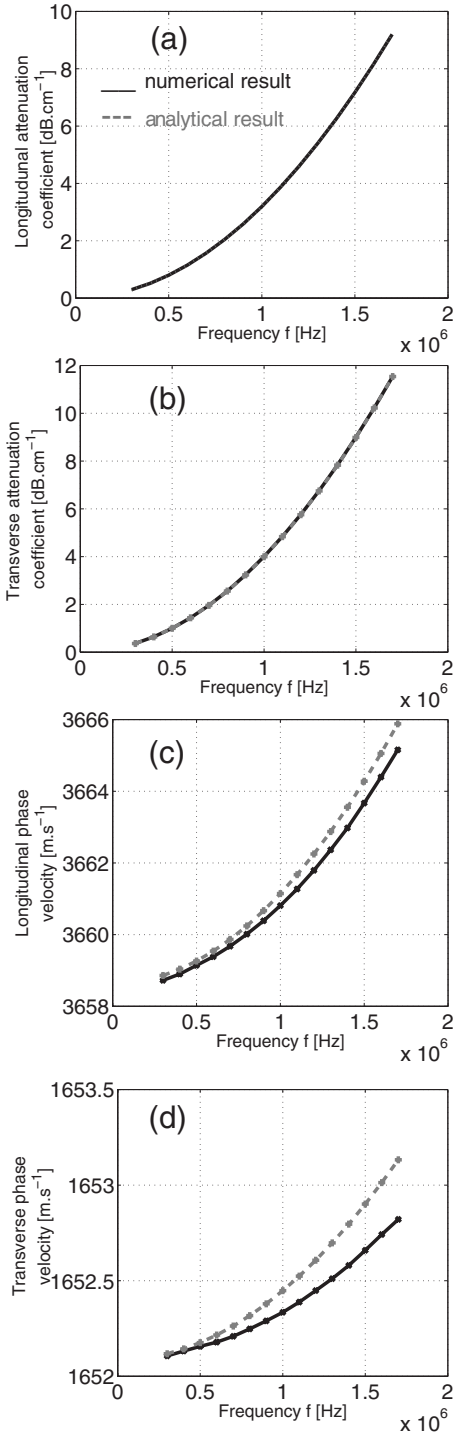

FIG. 3. Comparison between numerical (black solid lines) and analytical (gray dashed lines) results obtained for a plane wave propagation through an homogeneous transverse isotropic viscoelastic medium. [(a) and (b)] Attenuation coefficient of the longitudinal (transverse) wave mode. [(c) and (d)] Phase velocity of the longitudinal (transverse) wave mode. All velocities are plotted within the bandwidth of interest.

C. Effect of absorption on the first wavefront amplitude

In order to assess the qualitative effect of viscous properties of both fluids and of the viscoelastic properties of the solid on the FAS, Fig. 4 shows the amplitude of the first maximum of each signal recorded by the 14 receivers corresponding to the computation of the FAS velocity for a bone thickness equal to 4 mm. The amplitude of the signal at the first sensor with no attenuation was used to normalize the signals recorded at all the sensors in the elastic and viscoelastic case. The values of the components of the stiffness tensor were taken equal to their reference value indicated in Table II. The solid line corresponds to the normalized amplitude of the signal obtained without any absorption neither in the fluids nor in the solid. The dashed line corresponds to the

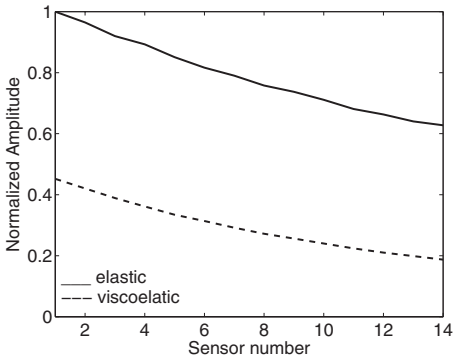

FIG. 4. Variation in the amplitude of the first arriving wave front as a function of the sensor number (increasing number corresponds to sensors farther to the emitter). The amplitude of the signal at the first sensor with no attenuation was used to normalize the signals recorded at all the sensors in the elastic and viscoelastic case. The values of the components of the stiffness tensor are equal to the reference values indicated in Table I. The solid line indicates the results when no absorption was accounted for and the dashed line indicates the case where viscous losses are considered in both surrounding fluids as well as in the solid (reference values indicated in Table III are used for viscous and viscoelastic parameters).

normalized amplitude of the signal obtained by considering absorption in both fluids and in the solid, the viscous and viscoelastic parameters being equal to their reference values given in Tables I and III.

The difference between the dashed and solid lines illustrates the influence of viscous and viscoelastic effects on the amplitude of the FAS. For both configurations (elastic and viscous cases), the amplitude of the signal is shown to decrease as a function of the position of the receiver, which can be explained by the fact that the wave radiates in fluid while it propagates in the bone structure, leading to a loss of energy. As shown in Fig. 4, including viscous and viscoelastic absorptions in the simulation model leads to a decrease in the amplitude of the first arriving wavefront.

When the reference material properties are considered, the FAS velocity obtained without absorption is equal to 3484 m s^{-1}, whereas it is equal to 3733 m s^{-1} when absorption is taken into account. The difference between these two values is significant, compared to the precision of the probe, and will be investigated in what follows.

D. Dependence of the FAS velocity to absorption in the surrounding fluids

From the analysis of numerical simulations, the variation in the FAS velocity due to changes of viscous properties of the soft tissues and of bone marrow within a realistic range was assessed for $h=0.6$ and 4 mm, and for homogeneous material properties. The material properties of cortical bone were taken equal to their reference values, as given in Table II for the stiffness tensor $\mathbb{C}$, and in Table III for the viscoelastic tensor $\mathbb{E}$. The minimal (m) and maximal (M) values of η_f are tested for the soft tissues and for bone marrow; the other material properties remaining equal to their reference values.

Table IV shows that the FAS velocity is independent of the viscous properties of the soft tissues, as well as of marrow within the physiological range. Therefore, the soft tissues and bone marrow will be considered as nonviscous fluids in what follows.

TABLE IV. Sensitivity of the FAS velocity to changes of the viscous properties of the soft tissues and of bone marrow for two values of the cortical thickness and homogeneous bone material properties. The computed FAS velocity is indicated for the minimal and maximal values of each variable corresponding to the realistic range of variation shown in Table II.

Material property S	η_f in soft tissues (Pa s)		η_f in bone marrow (Pa s)	
Cortical thickness h (mm)	0.6	4	0.6	4
FAS velocity for S_m (m s^{-1})	3483	3731	3484	3731
FAS velocity for S_M (m s^{-1})	3484	3732	3484	3731

E. Dependence of the FAS velocity to homogeneous viscoelastic absorption in cortical bone

The variation in the FAS velocity due to changes of the viscoelastic parameters of cortical bone within a realistic range was assessed for $h=0.6$ and 4 mm, and for homogeneous material properties, in order to determine which viscoelastic parameters play a role in the FAS velocity and must thus be considered to have spatial variations. Therefore, the material properties of the surrounding soft tissues and of the stiffness tensor were taken equal to their reference values, as indicated in Tables I and II. The minimal (m) and maximal (M) values of each component of the viscoelastic tensor $\mathbb{E}$ of cortical bone indicated in Table III were tested; the other material properties remaining equal to their reference values, except for C_{13}, which was taken equal to its minimum value when considering variations of C_{11} and C_{33} (in order to satisfy the thermodynamical stability conditions for all values, see Appendix). Table V shows the FAS velocity corresponding to a variation of each material property.

According to the value of h and to the considered viscoelastic property S, two situations may be distinguished: the difference of the FAS velocities obtained when considering the maximum and minimum values of S may be relatively "large" (above 67 m s^{-1}) or relatively "small" (lower than 3 m s^{-1}). Considering the thick solid layer ($h=4$ mm), Table V shows that small differences of the FAS velocity are obtained, when η_{13}, η_{33}, and η_{55} take their minimum or maximum values defined above. On the contrary, the FAS

TABLE V. Sensitivity of the FAS velocity to changes of the viscoelastic properties of cortical bone for two values of the cortical thickness and homogeneous bone material properties. The computed FAS velocity is indicated for the minimal and maximal values of each variable corresponding to the realistic range of variation shown in Table II.

Material property S	η_{11} (Pa s)		η_{13} (Pa s)		η_{33} (Pa s)		η_{55} (Pa s)	
Cortical thickness h (mm)	0.6	4	0.6	4	0.6	4	0.6	4
FAS velocity for S_m (m s^{-1})	3456	3654	3543	3738	3544	3732	3484	3734
FAS velocity for S_m (m s^{-1})	3787	3956	3475	3735	3469	3734	3484	3733

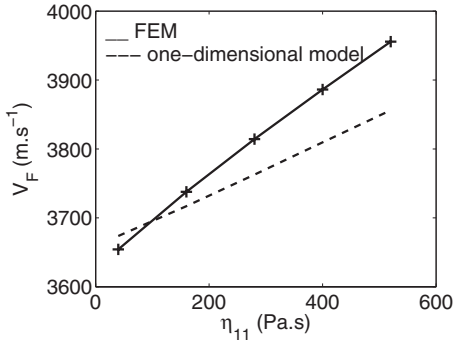

FIG. 5. Case of thick solid layer h=4 mm. Variation in the FAS velocity (v_F) versus η_{11} for homogeneous bone properties, the other material properties remaining equal to their reference value. The solid (respectively dashed) line indicates the results obtained using the finite element model (respectively the one-dimensional model described in subsection IV A)

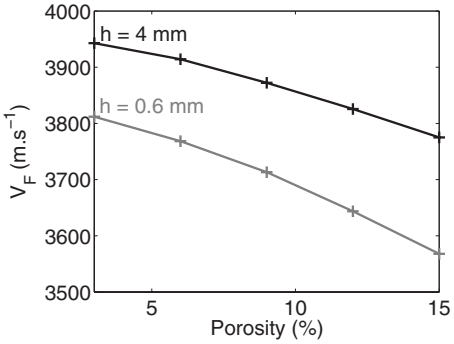

FIG. 7. Variation in the FAS velocity (v_F) versus porosity for homogeneous bone material properties. The black (respectively gray) solid line corresponds to the case of a thick (respectively thin) solid layer of h=4 mm (respectively, h=0.6 mm)

velocity varies significantly when η_{11} varies within the limits defined above. The solid line in Fig. 5 shows the variation in the FAS velocity as a function of η_{11} in the case of homogeneous bone properties; the other components of $\mathbb{E}$ and $\mathbb{C}$ remaining constant and equal to their reference value. The FAS velocity is shown to be an increasing function of η_{11} within the physiological range.

When considering the thin solid layer (h=0.6 mm), changes in η_{55} weakly affect the FAS velocity, while variations of η_{11}, η_{13}, and η_{33} lead to significantly larger changes of the FAS velocity. As shown in Fig. 6, the FAS velocity is an increasing function of η_{11} and η_{33}, and a decreasing function of η_{13} within the physiological range. The components of the viscoelastic tensor (η_{11}, η_{13}, and η_{33}), which influence the FAS velocity are the same than the components of the stiffness tensor (C_{11}, C_{13}, and C_{33}) having an effect on the FAS velocity (Haïat *et al.*, 2009) and determining the plate velocity v_p [see Eq. (6)].

Figure 7 shows the variation in the FAS velocity for homogeneous cortical bone where the porosity is assumed to vary within the physiological range, inducing a simultaneous variation in mass density and of all components of $\mathbb{C}$ and of $\mathbb{E}$. The results shown in Fig. 7 indicate that the FAS velocity is a decreasing function of the porosity for thick and thin bone widths, and that the dependence of the FAS velocity on the porosity is approximately similar for both thickness values.

In what follows, the effect of a gradient of each viscoelastic property playing a role in the determination of the FAS velocity will be investigated for both values of the bone thickness.

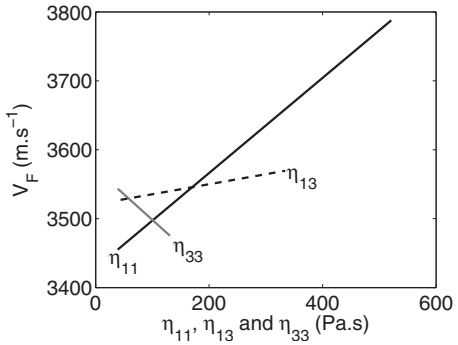

FIG. 6. Case of thin solid layer h=0.6 mm. Variation in the FAS velocity (v_F) *versus* η_{11} (black solid line), η_{13} (black dashed line) and η_{33} (gray solid line) for homogeneous bone properties, the other material properties remaining equal to their reference value.

F. Gradient of bone viscoelastic properties

1. A thick solid layer

Figure 8 shows the dependence of the FAS velocity on the gradient of η_{11} in the case of a thick solid layer (h=4 mm). For a gradient of type 1, the FAS velocity increases when δ_{11} increases, whereas for gradient of type 2, the FAS velocity slightly decreases with δ_{11}. The dashed lines of Fig. 8 describe the FAS velocity obtained for a constant value of η_{11} equal to its spatially averaged values, which corresponds to the value of η_{11} at z=−0.5h. The dashed lines of Fig. 8 were derived from the results shown in Fig. 5. The results indicate that in the case of a thick bone width with heterogeneous bone properties, an important dis-

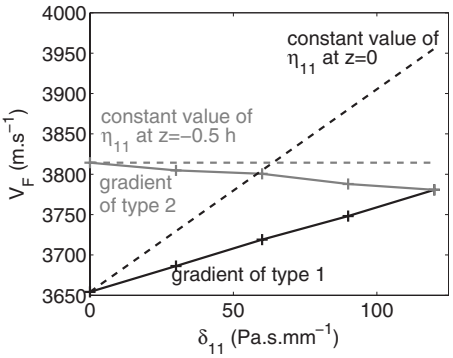

FIG. 8. Case of thick solid layer h=4 mm. Variation in the FAS velocity (v_F) *versus* δ_{11}. The black lines correspond to the variation in type 1 (constant value of η_{11} at z=0) and the gray lines correspond to the variation in type 2 (constant value of η_{11} at z=−0.5h). The continuous lines indicate the results obtained with the finite element model. The dashed lines correspond to the FAS velocity obtained with homogeneous spatially averaged viscoelastic properties (corresponding to the value at z=−0.5h) obtained from Fig. 5.

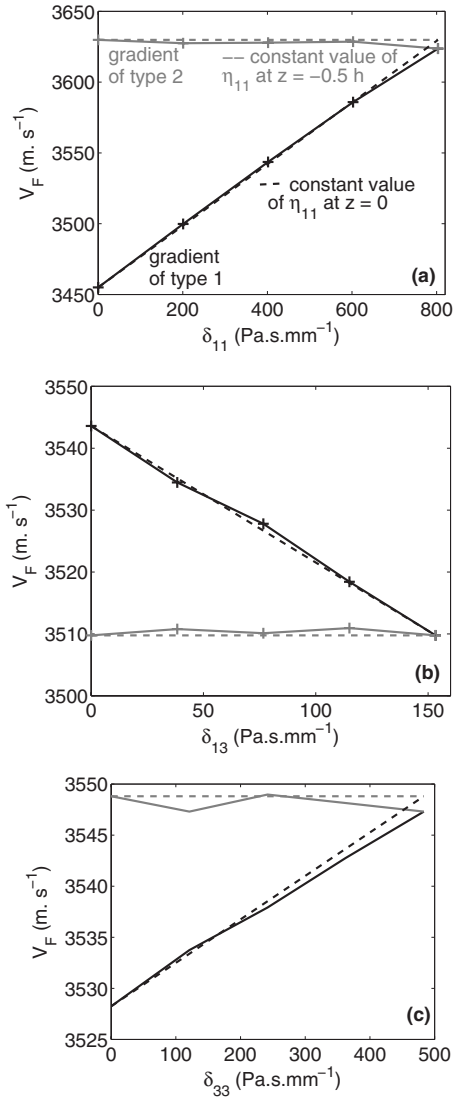

FIG. 9. Case of thin solid layer h=0.6 mm. Variation in v_F versus (a) δ_{11}, (b) δ_{33} and (c) δ_{13}. The black lines correspond to the variation in type 1 (constant value of η_{11}, η_{33} and η_{13} at z=0) and the gray lines correspond to the variation in type 2 (constant value of η_{11}, η_{33} and η_{13} at z=−0.5h). The continuous lines indicate the results obtained with the finite element model. The dashed lines correspond to the FAS velocity obtained with homogeneous spatially averaged viscoelastic properties (corresponding to the value at z=−0.5h)

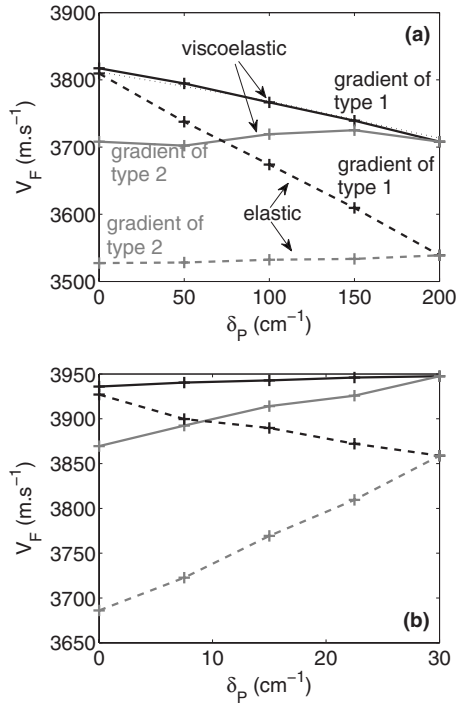

FIG. 10. Variation in v_F versus porosity for (a) h=0.6 mm and (b) h=4 mm. The black lines correspond to the variation in type 1 (constant value of P at z=0) and the gray lines correspond to the variation in type 2 (constant value of P at z=−0.5h). The solid lines indicate the results obtained when considering a simultaneous variation in mass density and of the stiffness and viscoelastic coefficients. The dashed lines indicate the results obtained when considering a simultaneous variation in mass density and of the stiffness coefficients only, bone being considered as an elastic material (see Haïat *et al.* (2009)). The thin dotted line in Fig. 10(a) shows the FAS velocity obtained when considering a constant value of the porosity equal to its spatially averaged values, which corresponds to the value of the porosity at z=−0.5h. (This line is very near to the black line.)

crepancy is obtained when comparing the numerical results and the FAS velocity obtained by spatially averaging η_{11} across the bone width.

2. A thin solid layer

When considering the thin solid layer (h=0.6 mm), the effect of a gradient of η_{11}, η_{13}, and η_{33} was investigated according to the results presented in Sec. III E. The results are shown in Fig. 9.

For a gradient of type 1, the FAS velocity is shown to increase when δ_{11} and δ_{33} increase, whereas it decreases when δ_{13} increases. For a gradient of type 2, the FAS velocity stays approximately constant with δ_{11}, δ_{13}, and δ_{33}.

The dashed lines of Fig. 9 show the FAS velocity obtained for a constant values of η_{11}, η_{33}, and η_{13} equal to their spatially averaged values, which correspond to the values of η_{11}, η_{33}, and η_{13} at z=−0.5h. The dashed lines of Fig. 9 were derived by considering the results shown in Fig. 5. For both types of gradient, the FAS velocity is accurately predicted by considering the spatially averaged values of η_{11}, η_{33}, and η_{13}, which shows that in the case of a thin bone width with heterogeneous bone properties; the FAS velocity is governed by the spatially averaged values of the viscoelastic properties η_{11}, η_{13}, and η_{33}.

G. Gradient of porosity

Figures 10(a) and 10(b) show the variation in the FAS velocity obtained for h=0.6 and 4 mm, respectively, when considering a gradient of porosity δ_P. The black and gray solid lines show the FAS velocity obtained numerically for a gradient of porosity of types 1 and 2, respectively. Note that the porosity induces a variation in mass density, as well as of the stiffness and viscoelastic coefficients, as described in Sec. II D. The dashed lines of Fig. 10 are the results described by Haïat *et al.* (2009), corresponding to the results obtained by only accounting for variations of stiffness coefficients and of mass density due to changes of porosity (elastic case).

As shown in Fig. 10, the viscoelastic behavior of cortical bone induces an increase in the FAS velocity compared to the elastic case. In the case of a thin bone width [Fig. 10(a)],

the FAS velocity does not depend on δ_P for a gradient of type 2, which is a result similar to what has been obtained in the elastic case. However, for a gradient of type 1, the FAS velocity decreases with δ_P with a slope approximately divided by 2, compared to the elastic case. The dashed line in Fig. 10(a) shows the FAS velocity obtained for a constant value of the porosity equal to its spatially averaged values, which corresponds to the value of the porosity at $z=-0.5h$. A good agreement is obtained between the results found with a gradient and with spatially averaged material properties, which confirms that in the case of a thin bone width with heterogeneous porosity, the FAS velocity is governed by the spatially averaged values of the porosity.

In the case of a thick bone width [see Fig. 10(b)], the FAS velocity increases with δ_P for a gradient of type 2, with a slope slightly lower than what is obtained in the elastic case. However, for a gradient of type 1, the FAS velocity slightly increases with δ_P, whereas it decreases with δ_P in the elastic case.

IV. DISCUSSION

To the best of our knowledge, this study is the first one to focus on the effect of ultrasonic attenuation on the FAS velocity estimated with an axial transmission configuration for different solid layer thicknesses.

The present study shows that in the studied geometrical configuration, ultrasonic attenuation effects related to the surrounding soft tissues are not likely to modify the results compared to the case with no losses. However, as shown in Fig. 4, attenuation effects strongly influence the amplitude of the signal associated with the FAS velocity. Our results show that in the case of bone with strong attenuation, the amplitude of the FAS may be significantly reduced compared to the elastic case (a factor of 3 may be expected). In some situations of strong bone attenuation, this decrease might lead to wrong estimation of the time of the FAS if the FAS amplitude does not cross the threshold used for the determination of the FAS, which is more likely for the receivers located far from the emitter because losses of amplitude are comparatively more important.

The results shown in Table V suggest that the effect of changes of viscoelastic properties within their estimated physiological range may be of the same order of magnitude as the effect of changes of the stiffness coefficients or mass density within the physiological range (Haïat *et al.*, 2009). These results indicate that attenuation is an important property, which should be accounted for when modeling the ultrasonic propagation in cortical bone in the context of axial transmission. Moreover, for both thin and thick bone widths, the components of the viscoelastic tensor affecting the FAS velocity are the same as the components of the elastic tensor influencing the value of the FAS velocity found in Table II of Haïat *et al.* (2009).

A. A one-dimensional model

To understand the results shown in Figs. 5 and 6, a one-dimensional model using linear filters similar to what has been developed by Haïat *et al.* (2006) has been applied. This model corresponds to a 1-D model in a viscoelastic medium where bone thickness is not taken into account. The approach is based on results obtained in trabecular bone showing that speed of sound values measured using a time marker in the early part of the signal increases when BUA increases (Haïat *et al.*, 2005, 2006; Wear, 2000, 2001).

Briefly, we employed a linear filter with a quadratic frequency dependent attenuation coefficient in order to generate 14 radio frequency signals on which the FAS velocity will be estimated using the model described in Sec. II A. Signal simulation was performed in order to understand the effects of the frequency dependent attenuation coefficient on the velocity measurements. For a given quadratic frequency dependent attenuation coefficient in bone $\alpha(f)=\beta f^2$, a transfer function was determined so that the effect of the propagation in bone could be modeled as a quadratic filter. In this last relation, β is a constant, consistently with the constant value of the viscoelastic coefficients.

In the model, the simulated signal $s_s(t)$ [with Fourier transform $S_s(f)$], corresponding to a propagation in bone over a distance of L, was obtained using the emitted signal $e(t)$ [Fourier transform $E(f)$] through

$$S_s(f) = E(f)\exp(-\beta f^2 L)\exp\left(-2i\pi f\frac{L}{v_{L,x}^{\phi}(f)}\right), \tag{15}$$

where the transfer function $H_1(f)=\exp(-\beta f^2 L)$ accounts for the attenuation in bone (attenuation in water was taken to be negligible as it does not impact the FAS velocity), and $H_2(f)=\exp(-2i\pi f(L/v_{L,x}^{\phi}(f)))$ accounts for the time delay corresponding to the propagation in bone. Following Eqs. (A3) and (A4) (see Appendix), together with the expression of the attenuation coefficient, we have

$$v_{L,x}^{\phi}(f) = c_{L,x}\left(1+\frac{3}{8\pi^2}c_{L,x}^2\beta^2 f^2\right). \tag{16}$$

For each value of β, the approach described above allows to construct a set of 14 signals by varying the value of L accordingly to the position of the receivers. A value of $L=0$ was arbitrarily chosen for the receiver located at the left of Fig. 1. Note that choosing another value would not impact the results presented below, as the FAS velocity is derived from the comparison between the 14 receivers and does not depend on the shape of the first signal. The FAS velocity was derived, following the same method, as described in Sec. II A.

The relationship between the parameter β and the bone viscoelastic properties depends on the bone thickness considered. In the case of a large bone thickness, the situation is relatively simple because only η_{11} impacts the FAS velocity, and using Eq. (A3) leads to

$$\beta = 2\pi^2\frac{\eta_{11}}{c_{L,x}C_{11}}. \tag{17}$$

The dashed line of Fig. 5 shows the variation in the FAS velocity as a function of η_{11} in the case of the 1-D model described above. The dashed line of Fig. 5 does not correspond to the "correct value" of the FAS velocity, and the solid line (results obtained with the 2-D simulation method)

reflects more closely the reality. Despite the strong approximation performed in the 1-D model (dashed line) compared to the 2-D model (solid line), a reasonable agreement is obtained between both methods as the maximum difference between both velocities is equal to 100 m s^{-1}. The distortion due to dispersion and the use of the time at which the peak of the FAS occurs is included in both 1-D and 2-D models. Note that similar results are obtained in the case of a thin bone width (data not shown) when considering an isotropic behavior ($\mathbb{C}$ and $\mathbb{E}$ isotropic tensors), which is necessary in order to derive an analytical relationship between β and the bone material properties.

B. Limitations

This study has limitations. First, the determination of homogenized viscoelastic material properties of cortical bone is a complex problem due to the multiscale nature of bone. Bone material properties depend on the microstructure (*e.g.* porosity, shape, and distribution of the pores), as well as on the material properties of the bone matrix at smaller scales (*e.g.* mineralization, orientation of collagen fibrils, etc.). Both porosity and material properties of bone tissue may depend on the radial position in bone and result in a gradient of all components of $\mathbb{C}$, $\mathbb{E}$, and in ρ_s. Therefore, multiscale models, coupled with structural and stiffness measurements at lower scales 9such as nanoindentation (Zysset *et al.*, 1999) or scanning acoustic microscopy (Raum *et al.*, 2006)] are needed in order to derive more realistic spatial variations in homogenized material properties.

Second, although the range of variation chosen for each component of the viscoelastic tensor was determined from the experimental results obtained by the group of some of the authors (Sasso *et al.*, 2007, 2008) for bovine cortical bone samples at 4 MHz, the precise relationship between the attenuation coefficient and porosity in human cortical bone around 1 MHz remains poorly understood. The values of η_{11} and η_{33} were obtained by considering BUA values measured at 4 MHz, and a linear dependence of the attenuation coefficient between 0 and 4 MHz. However, the dependence of the attenuation coefficient has been shown to be slightly nonlinear over a wide frequency bandwidth [see Fig. 5 of Sasso *et al.* (2007)]. Moreover, as shown by Eq. (A3), our time model approximation leads to a f-square dependence of the attenuation coefficient, which is not necessarily the case for real cortical bone samples. In order to account for other frequency dependence of the attenuation coefficient in the framework of a time-domain model, would need to be used, similarly as what was done in fluids using a fractional time derivative (Wismer, 2006) or a causal convolution wave equation (Cobbold *et al.*, 2004). However, the frequency dependence of the attenuation coefficient in cortical bone remains poorly understood. Ultrasonic attenuation has been shown to be related to scattering effects due to the presence of the pores (Sasso *et al.*, 2008). However, viscoelastic properties of the bone matrix are also expected to influence ultrasonic attenuation, but this dependence remains to be quantified. The coupling of scattering and viscous absorption effects makes the prediction of the frequency dependence of the attenuation coefficient difficult. The development of homogenization models capable of predicting bone attenuation and/or dispersive effects would be of great interest to predict the evolution of bone ultrasonic response with material properties or thickness.

Third, this study was performed in two dimensions, and this analysis would need to be validated in 3D and taking into account also the heterogeneity of cortical thickness and true varying 3D shape of the bone. However, it has been shown by Bossy *et al.* (2004b) that 2-D and 3-D simulations give qualitatively similar results.

Fourth, the linear dependence of the material properties as a function of the position (gradient of types 1 and 2) in the bone cross-section chosen in this study corresponds to a simple situation compared to the physiological situation. We choose this linear variation because the precise spatial variations of bone material properties remain poorly documented. Moreover, this model constitutes a first step toward the determination of the effect of more realistic spatial dependence of material properties. In a forthcoming paper, we have used homogenization models, coupled with high resolution imaging techniques to show that each material property varies approximately linearly as a function of the radial position. Further work should use the results obtained in this way to account for more realistic spatial variations of bone material properties.

ACKNOWLEDGMENT

This study was supported by the "Agence Nationale de la Recherche" (Contract BoneChar No. BLAN06-2_144779).

APPENDIX: PHYSIOLOGICAL MATERIAL PROPERTIES

1. Attenuation in the surrounding soft tissues

The mechanical properties of both fluid layers (soft tissues and bone marrow) were considered to be homogeneous. We assumed constant values for the mass density $\rho_f = 1$ g cm^{-3} and the compressibility $K = 2.25 \times 10^9$ Pa corresponding to an acoustic wave velocity c_f of 1 500 m s^{-1} in the absence of viscosity ($\eta_f = 0$) (El Sariti *et al.*, 2006).

The attenuation coefficient α_f is assumed to have a square frequency dependence, and writes (Auld, 1973; Royer and Dieulesaint, 2000)

$$\alpha_f = \frac{1}{2}\frac{\eta_f}{c_f K}\omega^2, \tag{A1}$$

when the condition $\omega \gg \alpha_f c_f$ is fulfilled, where $\omega = 2\pi f$ is the angular frequency and f the frequency. Note that at the center frequency of 1 MHz, $\omega \sim 6.3 \times 10^6$ s^{-1} and $\alpha_f c_f \sim 1.4 \times 10^5$ s^{-1}. Moreover, the phase velocity v^ϕ is given by Auld (1973) or Royer and Dieulesaint (2000):

$$v^\phi = c_f\left(1 + \frac{3}{8}\frac{\eta_f^2}{K^2}\omega^2\right). \tag{A2}$$

2. Stiffness tensor of cortical bone

In order to define realistic numerical values for the different components of the stiffness tensor of cortical bone and for their variation, the same approach as the one described by Haïat *et al.* (2009) is used in the present work. Here, we assume that cortical bone is transverse isotropic, as this approximation has been shown to be realistic experimentally by different authors (Bossy *et al.*, 2004b; Dong and Guo, 2004; Haïat *et al.*, 2009; Protopappas *et al.*, 2007; Yoon and Katz, 1976a, 1976b). The values of the stiffness coefficients corresponding to the mean values of the bone mechanical properties are referred to as "reference" set of parameters in what follows. The porosity was assumed to vary between 3% and 15% (Bousson *et al.*, 2001; Dong and Guo, 2004), and a rule of mixture leads to the range of variation in mass density.

3. Attenuation in cortical bone

The attenuation coefficients $\alpha_{L,x}$ and $\alpha_{L,z}$ associated with the longitudinal mode are respectively given in the x-axis and z-axis by Auld (1973) or Royer and Dieulesaint (2000):

$$\alpha_{L,x} = \frac{1}{2}\frac{\eta_{11}}{c_{L,x}C_{11}}\omega^2, \quad \alpha_{L,z} = \frac{1}{2}\frac{\eta_{33}}{c_{L,z}C_{33}}\omega^2, \tag{A3}$$

when the conditions $\omega \gg \alpha_{L,x}c_{L,x}$ and $\omega \gg \alpha_{L,z}c_{L,z}$ are fulfilled, respectively, where $c_{L,x}=\sqrt{C_{11}/\rho_s}$ and $c_{L,z}=\sqrt{C_{33}/\rho_s}$. Note that at the center frequency of 1 MHz, $\omega \sim 6.3\times 10^6$ s^{-1} and $\alpha_{L,x}c_{L,x} \sim 8.3\times 10^4$ s^{-1}.

Under these conditions, the associated phase velocities $v_{L,x}^{\phi}$ and $v_{L,z}^{\phi}$ are respectively given by

$$v_{L,x}^{\phi} = c_{L,x}\left(1+\frac{3}{8}\frac{\eta_{11}^2}{C_{11}^2}\omega^2\right), \quad v_{L,z}^{\phi} = c_{L,z}\left(1+\frac{3}{8}\frac{\eta_{33}^2}{C_{33}^2}\omega^2\right). \tag{A4}$$

Similarly, the attenuation coefficient α_T associated with the transverse mode is given in the x-axis by Auld (1973) or Royer and Dieulesaint (2000):

$$\alpha_T = \frac{1}{2}\frac{\eta_{55}}{c_T C_{55}}\omega^2, \tag{A5}$$

when the condition $\omega \gg \alpha_T c_T$ is fulfilled, where $c_T=\sqrt{C_{55}/\rho_s}$. Note that at the center frequency of 1 MHz, $\omega \sim 6.3\times 10^6$ s^{-1} and $\alpha_T c_T \sim 1.7\times 10^4$ s^{-1}.

Under this condition, the transverse phase velocity v_T^{ϕ} is given by

$$v_T^{\phi} = c_T\left(1+\frac{3}{8}\frac{\eta_{55}^2}{C_{55}^2}\omega^2\right). \tag{A6}$$

The values of η_{11}, η_{33}, and η_{55} are assumed to be constant within the frequency bandwidth of interest and determined by the value of α_f when $f_0=1$ MHz. The approximation of constant values for the viscoelastic constants corresponds to a dispersive medium, as indicated by Eqs. (A6) and (A4).

We could not find in the literature a simple way to determine the value of η_{13}. Therefore, the reference value of η_{13} is derived from the mean values of η_{11} and η_{55} by assuming an isotropic behavior of viscoelasticity, which leads to the relation

$$\eta_{13} = \eta_{11} - 2\eta_{55}. \tag{A7}$$

In addition, the minimum and maximum values of η_{13} were obtained by verifying that the following positive-definiteness properties (so-called thermodynamical stability conditions) (Ohayon and Soize, 1998):

$$\eta_{11} > 0, \quad \eta_{33} > 0, \quad \eta_{55} > 0, \quad -\eta_{13}^2 + \eta_{11}\eta_{33} > 0, \tag{A8}$$

is always respected when varying each material property independently within the physiological range. This approach constitutes a simple way of determining a realistic range of variation for η_{13}. The physiological ranges of variation in the other viscoelastic constants (η_{11}, η_{33}, and η_{55}, respectively) are obtained by considering the different values of ultrasonic attenuation coefficient measured in the literature, and using Eqs. (A3) and (A5), respectively. So, we have considered a spatial variation in the different viscoelastic properties within this range of variation.

Ammann, P., and Rizzoli, R. (**2003**). "Bone strength and its determinants," Osteoporosis Int. **14**, S13–S18.

Auld, B. A. (**1973**). *Acoustic Fields and Waves in Solids* (Wiley Interscience, New York).

Baron, C., Talmant, M., and Laugier, P. (**2007**). "Effect of porosity on effective diagonal stiffness coefficients (c_{ii}) and anisotropy of cortical at 1 MHz: A finite-difference time domain study," J. Acoust. Soc. Am. **122**, 1810–1817.

Bossy, E., Talmant, M., and Laugier, P. (**2002**). "Effect of bone cortical thickness on velocity measurements using ultrasonic axial transmission: A 2D simulation study," J. Acoust. Soc. Am. **112**, 297–307.

Bossy, E., Talmant, M., and Laugier, P. (**2004a**). "Bi-directional axial transmission can improve accuracy and precision of ultrasonic velocity measurement in cortical bone: A validation on test material," IEEE Trans. Ultrason. Ferroelectr. Freq. Control **51**, 71–79.

Bossy, E., Talmant, M., and Laugier, P. (**2004b**). "Three-dimensional simulations of ultrasonic axial transmission velocity measurement on cortical bone models," J. Acoust. Soc. Am. **115**, 2314–2324.

Bossy, E., Talmant, M., Peyrin, F., Akrout, L., Cloetens, P., and Laugier, P. (**2004c**). "An *in vitro* study of the ultrasonic axial transmission technique at the radius: 1-MHz velocity measurements are sensitive to both mineralization and intracortical porosity," J. Bone Miner. Res. **19**, 1548–1556.

Bousson, V., Meunier, A., Bergot, C., Vicaut, E., Rocha, M. A., Morais, M. H., Laval-Jeantet, A. M., and Laredo, J. D. (**2001**). "Distribution of intracortical porosity in human midfemoral cortex by age and gender," J. Bone Miner. Res. **16**, 1308–1317.

Cobbold, R., Sushilov, N., and Weathermon, A. (**2004**). "Transient propagation in media with classical or power-law loss," J. Acoust. Soc. Am. **116**, 3294–303.

COMSOL Multiphysics (**2005**). Model library, Grenoble (France).

Desceliers, C., Soize, C., Grimal, Q., Haïat, G., and Naili, S. (**2008**). "Three dimensional transient elastic waves in multilayer semi-infinite media solved by a time-space-spectral numerical method," Wave Motion **45**, 383–399.

Dong, X. N., and Guo, X. E. (**2004**). "The dependence of transversely isotropic elasticity of human femoral cortical bone on porosity," J. Biomech. **37**, 1281–1287.

Dussik, K., and Fritch, D. (**1956**). "Determination of sound attenuation and sound velocity in the structure constituting the joints, and of the ultrasonic field distribution with the joints of living tissues and anatomical preparations, both in normal and pathological conditions," Technical Report, Progress Report to Public Health Service, National Institutes of Health Project A454, Bethesda, MD.

El-Sariti, A., Evans, J., and Truscott, J. (**2006**). "The temperature dependence of the speed of sound in bovine bone marrow at 750 kHz," Ultra-

sound Med. Biol. **32**, 985–989.
Fritsch, A., and Hellmich, C. (**2007**). "'Universal' microstructural patterns in cortical and trabecular, extracellular and extravascular bone materials: Micromechanics-based prediction of anisotropic elasticity," J. Theor. Biol. **244**, 597–620.
Garcia, B. J., Cobbold, R. S. C., Foster, F. S., and McNeill, K. G. (**1978**). "Ultrasonic attenuation in bone," in *Proceedings of the IEEE Ultrasonic Symposium* (IEEE, Cherry Hill, NJ), pp. 327–330.
Goss, S., Johnston, R., and Dunn, F. (**1978**). "Comprehensive compilation of empirical ultrasonic properties of mammalian tissues," J. Acoust. Soc. Am. **64**, 423–457.
Grimal, Q., and Naili, S. (**2006**). "A theoretical analysis in the time-domain of wave reflection on a bone plate," J. Sound Vib. **298**, 12–29.
Haïat, G., Lhemery, A., Renaud, F., Padilla, F., Laugier, P., and Naili, S. (**2008a**). "Velocity dispersion in trabecular bone: Influence of multiple scattering and of absorption," J. Acoust. Soc. Am. **124**, 4047–4058.
Haïat, G., Naili, S., Grimal, Q., Talmant, M., Desceliers, C., and Soize, C. (**2009**). "Influence of a gradient of material properties on ultrasonic wave propagation in cortical bone: Application to axial transmission," J. Acoust. Soc. Am. **125**, 4043–4052.
Haïat, G., Padilla, F., Barkmann, R., Dencks, S., Moser, U., Glüer, C., and Laugier, P. (**2005**). "Optimal prediction of bone mineral density with ultrasonic measurements in excised human femur," Calcif. Tissue Int. **77**, 186–92.
Haïat, G., Padilla, F., Cleveland, R., and Laugier, P. (**2006**). "Effects of frequency dependent attenuation and dispersion on different speed of sound measurements on human intact femur," IEEE Trans. Ultrason. Ferroelectr. Freq. Control **53**, 39–51.
Haïat, G., Sasso, M., Naili, S., and Matsukawa, M. (**2008b**). "Ultrasonic velocity dispersion in bovine cortical bone: An experimental study," J. Acoust. Soc. Am. **124**, 1811–1821.
Han, S., Rho, J., Medige, J., and Ziv, I. (**1996**). "Ultrasound velocity and broadband attenuation over a wide range of bone mineral density," Osteoporosis Int. **6**, 291–296.
Hans, D., Srivastav, S. K., Singal, C., Barkmann, R., Njeh, C. F., Kantorovich, E., Gluer, C. C., and Genant, H. K. (**1999**). "Does combining the results from multiple bone sites measured by a new quantitative ultrasound device improve discrimination of hip fracture?," J. Bone Miner. Res. **14**, 644–651.
Lakes, R. S., Yoon, H. S., and Katz, J. L. (**1986**). "Ultrasonic wave propagation and attenuation in wet bone," J. Biomed. Eng. **8**, 143–148.
Langton, C. M., Ali, A. V., Riggs, C. M., Evans, J. A., and Bonfield, W. (**1990**). "A contact method for the assessment of ultrasonic velocity and broadband attenuation in cortical and cancellous bone," Clin. Phys. Physiol. Meas. **11**, 243–249.
Lees, S., and Klopholz, D. Z. (**1992**). "Sonic velocity and attenuation in wet compact cow femur for the frequency range 5 to 100 MHz," Ultrasound Med. Biol. **18**, 303–308.
Lehman, J., and Johnson, E. (**1958**). "Some factors influencing the temperature distribution in thighs exposed to ultrasound," Arch. Phys. Med. Rehabil. **39**, 347–356.
Macocco, K., Grimal, Q., Naili, S., and Soize, C. (**2005**). "Probabilistic modelling of an ultrasonic setup: Calculation of the dispersion on wave speed measurements," C. R. Mec. **333**, 565–573.
Macocco, K., Grimal, Q., Naili, S., and Soize, C. (**2006**). "Elastoacoustic model with uncertain mechanical properties for ultrasonic wave velocity prediction; application to cortical bone evaluation," J. Acoust. Soc. Am. **119**, 729–740.
Mayhew, P. M., Thomas, C. D., Clement, J. G., Loveridge, N., Beck, T. J., Bonfield, W., Burgoyne, C. J., and Reeve, J. (**2005**). "Relation between age, femoral neck cortical stability, and hip fracture risk," Lancet **366**, 129–135.
Muller, M., Moilanen, P., Bossy, E., Nicholson, P., Kilappa, V., Timonen, J., Talmant, M., Cheng, S., and Laugier, P. (**2005**). "Comparison of three ultrasonic axial transmission methods for bone assessment," Ultrasound Med. Biol. **31**, 633–642.
Ohayon, R., and Soize, C. (**1998**). *Structural Acoustic and Vibration* (Academic, San Diego).
Protopappas, V. C., Kourtis, I. C., Kourtis, L. C., Malizos, K. N., Massalas, C. V., and Fotiadis, D. I. (**2007**). "Three-dimensional finite element modeling of guided ultrasound wave propagation in intact and healing long bones," J. Acoust. Soc. Am. **121**, 3907–3921.
Raum, K., Cleveland, R. O., Peyrin, F., and Laugier, P. (**2006**). "Derivation of elastic stiffness from site-matched mineral density and acoustic impedance maps," Phys. Med. Biol. **51**, 747–758.
Raum, K., Leguerney, I., Chandelier, F., Bossy, E., Talmant, M., Saied, A., Peyrin, F., and Laugier, P. (**2005**). "Bone microstructure and elastic tissue properties are reflected in QUS axial transmission measurements," Ultrasound Med. Biol. **31**, 1225–35.
Rico, H. (**1997**). "The therapy of osteoporosis and the importance of cortical bone," Calcif. Tissue Int. **61**, 431–432.
Royer, D., and Dieulesaint, E. (**2000**). *Elastic Waves in Solids. I: Free and Guided Propagation* (Springer-Verlag, Berlin).
Sasso, M., Haïat, G., Yamato, Y., Naili, S., and Matsukawa, M. (**2007**). "Frequency dependence of ultrasonic attenuation in bovine cortical bone: An in vitro study," Ultrasound Med. Biol. **33**, 1933–1942.
Sasso, M., Haïat, G., Yamato, Y., Naili, S., and Matsukawa, M. (**2008**). "Dependence of ultrasonic attenuation on bone mass and microstructure in bovine cortical bone," J. Biomech. **41**, 347–355.
Seeley, D. G., Browner, W. S., Nevitt, M. C., Genant, H. K., Scott, J. C., and Cummings, S. R. (**1991**). "Which fractures are associated with low appendicular bone mass in elderly women? The Study of Osteoporotic Fractures Research Group," Ann. Intern Med. **115**, 837–842.
Serpe, L., and Rho, J. (**1996**). "The nonlinear transition period of broadband ultrasound attenuation as bone density varies," J. Biomech. **29**, 963–966.
Stegman, M. R., Heaney, R. P., Travers-Gustafson, D., and Leist, J. (**1995**). "Cortical ultrasound velocity as an indicator of bone status," Osteoporosis Int. **5**, 349–353.
Talmant, M., Kolta, S., Roux, C., Haguenauer, D., Vedel, I., Cassou, B., Bossy, E., and Laugier, P. (**2009**). "*In vivo* performance evaluation of bi-directional ultrasonic axial transmission for cortical bone assessment," Ultrasound Med. Biol. **35**, 912–919.
Thomas, C. D., Feik, S. A., and Clement, J. G. (**2005**). "Regional variation of intracortical porosity in the midshaft of the human femur: age and sex differences," J. Anat. **206**, 115–125.
Turner, C. H. (**2002**). "Biomechanics of bone: determinants of skeletal fragility and bone quality," Osteoporosis Int. **13**, 97–104.
Warren, G., and Scott, W. (**1996**). "Numerical dispersion of higher order nodal elements in the finite-element method," IEEE Trans. Antennas Propag. **44**, 317–320.
Wear, K. A. (**2000**). "The effects of frequency-dependant attenuation and dispersion on sound speed measurements: applications in human trabecular bone," IEEE Trans. Ultrason. Ferroelectr. Freq. Control **47**, 265–273.
Wear, K. A. (**2001**). "A numerical method to predict the effects of frequency-dependent attenuation and dispersion on speed of sound estimates in cancellous bone," J. Acoust. Soc. Am. **109**, 1213–1218.
Weiss, M., Ben-Shlomo, A., Hagag, P., and M., R. (**2000**). "Reference database for bone speed of sound measurement by a novel quantitative multi-site ultrasound device," Osteoporosis Int. **11**, 688–696.
WHO Study Group (**1994**), "Assessment of fracture risk and its application to screening for postmenopausal osteoporosis," WHO Technical Report No. 843, World Health Organization, Geneva, Switzerland.
Wismer, M. (**2006**). "Finite element analysis of broadband acoustic pulses through inhomogenous media with power law attenuation," J. Acoust. Soc. Am. **120**, 3493–502.
Yoon, H. S., and Katz, J. L. (**1976a**). "Ultrasonic wave propagation in human cortical bone—I. Theoretical considerations for hexagonal symmetry," J. Biomech. **9**, 407–412.
Yoon, H. S., and Katz, J. L. (**1976b**). "Ultrasonic wave propagation in human cortical bone—II. Measurements of elastic properties and micro hardness," J. Biomech. **9**, 459–464.
Zysset, P., Guo, X., Hoffler, C., Moore, K., and Goldstein, S. (**1999**). "Elastic modulus and hardness of cortical and trabecular bone lamellae measured by nanoindentation in the human femur," J. Biomech. **32**, 1005–12.